Effect of Elastic Modulus Mismatch on the Contact Crack Initiation in Hard Ceramic Coating Layer

Kee Sung Lee*
Energy Materials Research Center, Korea Institute of Energy Research, Daejeon 305-343, Korea

Effect of elastic modulus mismatch on the contact crack initiation is investigated to find major parameters in designing desirable surface-coated system. Silicon nitride coated soft materials with various elastic modulus mismatch, $E_c/E_s=1.06\sim356$ are prepared for the analysis. Hertzian contact test is conducted for producing contact cracks and the acoustic emission detecting technique for measuring the critical load of crack initiation. The implication is that coating thickness and material strength are controllable parameters to prevent the initiation of contact cracks resulted from the elastic modulus mismatch in the hard ceramic coating layer on the soft materials.

Key Words : Contact Crack, Elastic Modulus Mismatch, Coating, Coating Thickness, Strength, Crack Initiation

1. Introduction

Hard ceramic coatings on soft materials such as metals and polymers exhibit superior thermal and mechanical resistance over substrate monolith materials. More recent researches are directed to develop a technology required to reliable, reproducible, and cost-competitive hard coatings (Knight et al., 1989; Swain and Mencik, 1994; Pajares et al., 1996a). Engineering ceramic is a candidate material for the surface-protective coating, because it possesses desirable thermal and mechanical properties (Seo and Lim, 2002). It protects the substrate from thermal stress, corrosion, oxidation, wear and damage. Disadvantage of the substrate materials can be overcome by the surface coating possessing much more improved mechanical properties (Kim et al., 2002). However, the hard surface layers subjected to residual stress or elastic modulus mismatch — elastic modulus ratio between the coating and the substrate layer, E_c/E_s — can cause another failure problem (Knight et al., 1989; Barlett and Maschio, 1995). Coating layers containing stress caused by thermal or elastic mismatch can be subjected by additional stress change. For instance, thin layers containing such large residual compressive stresses are susceptible to delamination or spalling (Evans and Hutchinson, 1984; Hutchinson and Suo, 1991). A failure phenomenon can be also occurred in complex manner during contacting with hard indenter on the coating layer above a critical force (Pajares et al., 1996b).

In general, when a hard spherical indenter is pressed on a flat surface of brittle material, the contact force produces a crack with cone shape geometry (Lawn, 1993). When the contact load exceeds a critical point, contact cracks can be initiated at the critical flaw from highly localized stress fields (Hertz, 1896; Frank and Lawn, 1967; Jin and Kim, 2000). As the contact load P increases to a critical value, P_c, that is, $P>P_c$, cone crack "C" as indicated in Fig. 1 is produced. More recent works show that transverse cracks

* **E-mail** : keeslee@kier.re.kr
TEL : +82-42-860-3414; **FAX** : +82-42-860-3133
Energy Materials Research Center, Korea Institute of Energy Research, Daejeon 305-343, Korea. (Manuscript **Received** February 21, 2003; **Revised** September 18, 2003)

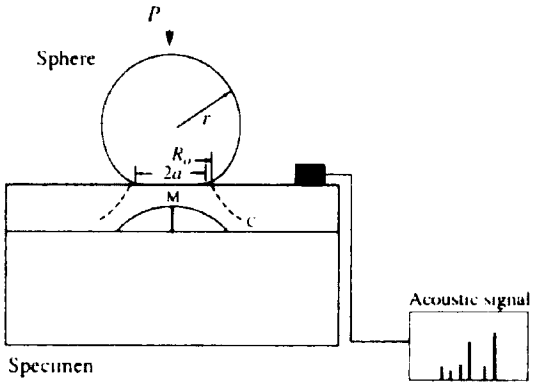

Fig. 1 Schematic diagram of contact tests. Typical cone crack (C) and transverse crack (M) are observed during contact with sphere indenter at load P. Tungsten carbide (WC) ball is indented on the flat surface. Contact radius a can be measured by optical microscope. Acoustic emission detector was attached on the flat surface of each specimen

(M indicated in the figure) can be initiated from the coating/substrate interface by contacting hard indenter on the coating layer (Pajares et al., 1996a ; Pajares et al., 1996b ; Wuttiphan et al., 1996). An elastic modulus mismatch between the coating and the substrate layer is particularly important in this contact, because the material is constrained during the contact. In other words, the elastic modulus is closely related with stress during the contact, particularly in hard materials such as ceramics.

Therefore, an investigation on the critical load of contact crack initiation from a point view of elastic modulus mismatch in the hard ceramic coating layer on a softer material is very important guideline to suggest important parameters in designing desirable surface-coated system. Two silicon nitride bilayers were prepared for the investigation of the effect of elastic modulus mismatch on the contact crack initiation. One is hard Si_3N_4 on soft Si_3N_4 system with different microstructure. As it consists of the same materials, there will be little elastic/plastic mismatch between the coating and the substrate layer. The other is Si_3N_4 on Si_3N_4+BN system. Boron nitride (BN) additions soften the substrate layer ; ultimately it induces the elastic modulus mismatch on the bilayers. The elastic modulus mismatch can be also controlled using by different glass or polymer substrate in this study. Thus, silicon nitride coated soft materials with elastic modulus mismatch, $E_c/E_s=1.06\sim356$ are prepared for the analysis. In any cases, they are prepared to have a strong interfacial bonding to exclude the effect of interfacial fracture during the contact. Hertzian contact tests and acoustic emission detecting techniques are used for inducing and detecting the contact cracks.

2. Experimental Method

2.1 Materials and fabrication

A common powder processing and firing procedure was used for the coating and the substrate layers, to ensure strong interlayer bonding in the finished product. The starting silicon nitride powers investigated in this study are fine α-Si_3N_4 (UBE-SN-E10, average particle size 0.3 μm Ube Industries America, NY) or coarse α-Si_3N_4 (UBE-SN-E3, average particle size 1 μm, Ube Industries America, NY). Sintering additives are 5 wt% Y_2O_3 (Fine Grade, H. C. Starck GmbH, Goslar, Germany), 2 wt% Al_2O_3 (AKP 50, Sumitomo Chemical Co. Ltd., Tokyo, Japan), and 1 wt% MgO (High Purity, Baikowski Co., N.C.). The Si_3N_4+BN compositions were prepared from the same fine Si_3N_4 powder (UBE-SN-E10, average particle size 0.3 μm Ube Industries America, NY), but with BN (Aldrich Chemical, Milwaukee, WI) additions of 5, 10, 20, 30 wt%.

The powders were mixed in isopropanol for 24 h in a planetary ball mill, using alumina balls in a propylene container. After drying, the softly agglomerated powder was crushed and sieved through a 60 mesh screen. The powders were hot pressed in a graphite mold of 50 mm diameter to form bilayer with coating thickness 1 mm and substrate thickness 3.5 mm or coating thickness 2 mm and substrate thickness 3.5 mm at 1700℃ ~ 1730℃ for 1hr in nitrogen at a pressure of 30 MPa. The powders for the coating and the substrate were illustrated in Table 1. The sintered disks were cut and machined into bar specimen

Table 1 Composition and elastic modulus of materials used in this study

Layer composition (wt%)		Elastic modulus (GPa)		Elastic modulus
coating	substrate	coating	substrate	mismatch, E_c/E_s
Si_3N_4(SN-E-3)	Si_3N_4(SN-E-10)	335	315	1.06
Si_3N_4(SN-E-10)	Si_3N_4(SN-E-10)+5BN	320	278	1.15
Si_3N_4(SN-E-10)	Si_3N_4(SN-E-10)+10BN	320	222	1.44
Si_3N_4(SN-E-10)	Si_3N_4(SN-E-10)+20BN	320	160	2.00
Si_3N_4(SN-E-10)	$47.4SiO_2+26.0MgO+14.2Al_2O_3+12.3BeO$	320	132	2.42
Si_3N_4(SN-E-10)	$47.6SiO_2+19.0CaO+9.5MgO+9.5BeO+9.5ZrO_2+48ZnO$	320	123	2.60
Si_3N_4(SN-E-10)	Si_3N_4(SN-E-10)+30BN	320	119	2.69
Si_3N_4(SN-E-10)	$38.1Al_2O_3+34.8CaO+8.1SiO_2+6.1ZrO_2+4.8B_2O_3+4.1BeO+4.0BaO$	320	109	2.94
Si_3N_4(SN-E-10)	$39.3Al_2O_3+36.0CaO+10.0B_2O_3+6.3ZrO_2+4.2BaO+4.2MgO$	320	103	3.11
Si_3N_4(SN-E-10)	$75.0SiO_2+15.0Na_2O+10.0CaO$	320	70	4.57
Si_3N_4(SN-E-10)	$96.6SiO_2+2.9B_2O_3+0.4Al_2O_3+0.02Na_2O$	335	68	4.71
Si_3N_4(SN-E-10)	$80.3SiO_2+12.2B_2O_3+4.0Na_2O+2.8Al_2O_3+0.4K_2O+0.3CaO$	320	62	5.16
Si_3N_4(SN-E-10)	$70.0PbO+30.0SiO_2$	320	44	7.27
Si_3N_4(SN-E-10)	$90.0B_2O_3+10.0SiO_2$	320	21	15.24
Si_3N_4(SN-E-10)	Acrylic polymer	335	5.2	61.54
Si_3N_4(SN-E-10)	Polycarbonate polymer	320	2.4	136.17
Si_3N_4(SN-E-10)	Soft polymer	320	0.9	355.56

with dimensions of 25 mm×4 mm×3 mm. Specimen surfaces normal to the hot-press direction were grinded maintaining coating thickness from 40 to 1250 μm, and then polished to 1 μm finish.

Glass or polymer supports with thickness of 12.5 mm were prepared as shown in Table 1. Elastic modulus was measured for each material using an acoustic apparatus (Grindosonic MK5, J. W. Lemmens Inc., U.S.A.). Upper coating layers were silicon nitride sintered layer of thickness $d=250$ μm. The heat treatment was performed at temperature above softening point of each substrate material to make a strong interfacial bonding. Thermal annealing was performed to generate negligible residual stresses during preparation. The products were cut and machined into bar specimen with dimensions of 25 mm× 4 mm×3 mm.

2.2 Contact test and characterization

Hertzian contact tests were made with a WC sphere of radius 1.98 mm (J&L Industrial Supply Co., MI, U.S.A.) at loads up to $P=3000$ N in a universal testing machine (Model 1122, Instron, Canton, U.S.A.), symmetrically across the interface between coating and substrate layer to test for delamination. The indentation damages were observed in Nomarski illumination of optical microscope.

Indentation stress-strain curves were obtained in order to evaluate the elastic modulus mismatch on the top surfaces of individual coating and substrate, using WC spherical indenters of radii $r=1.21\sim12.7$ mm at loads up to $P=4000$ N. For these tests, it was useful to coat the top surfaces with a gold film before indentation, to make the residual contact impressions visible in Nomarski illumination. From measurements of contact radius a in Fig. 1 at each value of P and r, indentation stress, $p_0=P/\pi a^2$, and indentation strain, a/r, could be evaluated, enabling construction of the stress-strain curves. To observe the yield stress, Y, a sequence of indentations with WC spherical indenters on the polished surfaces with a wide range of indentation loads. The indentation sites were considered to avoid damage interaction.

Acoustic emission experiments were performed on each coated material systems to evaluate the cone crack initiation load, P_c, during indentation at loads up to $P=4500$ N, using WC sphere radius $r=1.98$ mm. Schematic diagram is set up as shown in Fig. 1. The hard tungsten carbide (WC) sphere is contacted with flat surface of

hard coating layer. The intensity is recorded during loading-unloading cycle using a piezoelectric transducer (LOCAN320, Physical Acoustics, Princeton, U.S.A.) fixed on the surface of each specimen.

The other set of contact tests were made symmetrically along the traces of the interfaces on the top surfaces in the bonded-specimen, using WC spheres of radius $r=1.98$ mm at a fixed load. After separating the indented specimen halves in solvent, a gold coat was applied to the side surfaces for viewing in Nomarski contrast to confirm the initiation of contact cracks.

Finite element modeling (FEM) of stresses during the contact tests was carried out using a commercial package (Strand, G&D Computing, Sydney, Australia). The algorithm consists of a sphere of specified radius in axisymmetric frictionless contact on the flat coating layers. The maximum stress was calculated from corresponding point-by-point computations of the principal stresses below the contact.

3. Results and Discussion

Hertzian contact test across the coating/substrate interface was made to investigate the delamination of interface. Figure 2 shows the representative contact damages across the interface made on the polished section of the side in the hard Si_3N_4 on soft Si_3N_4 ($E_c/E_s=1.06$, Fig. 2 (a)) and the Si_3N_4 on Si_3N_4+30 wt%BN ($E_c/E_s=2.69$, Fig. 2(b)), at high load, $>P=2000$ N. No interface delamination in the contact test indicates that the interfaces of prepared specimens are strong enough (Evans and Hutchinson, 1984; Wuttiphan et al., 1996). All specimens studied in this study did not show any interface delamination. It is expected that contact forces can be applied to the substrate at high load because new surface energy will not be created. It means that the contact cracks are influenced sufficiently by the effect of the substrate during the contact in this study. It is noteworthy that the contact cracks are suppressed in the substrate part while a Hertzian crack appeared in the coating layer. The residual depression at the contact area of the

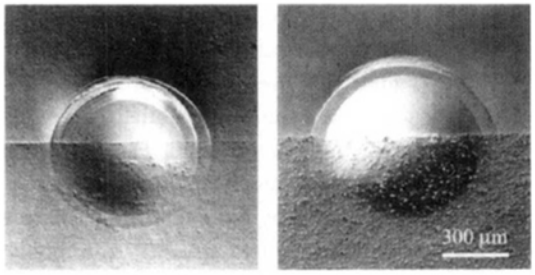

Fig. 2 Hertzian indentation damage on the side surface of Si_3N_4 coated material, made symmetrically across interface, (a) in hard Si_3N_4 on soft Si_3N_4 at $P=3000$ N, and (b) in Si_3N_4 on Si_3N_4+30 wt%BN at $P=2500$ N

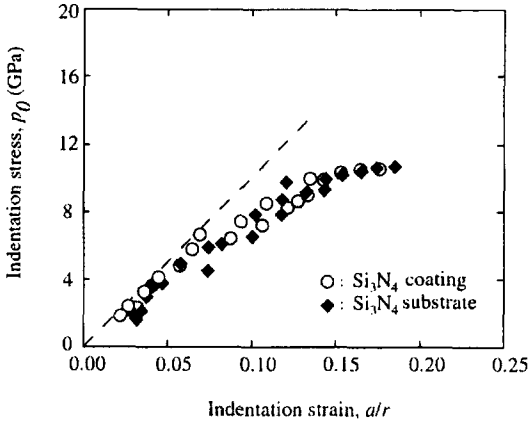

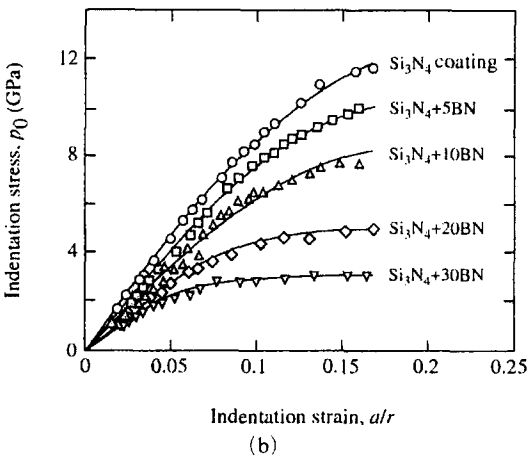

Fig. 3 Indentation stress-strain curves for each layer material used in (a) hard Si_3N_4 on soft Si_3N_4 and (b) Si_3N_4 on Si_3N_4+BN

substrate is found instead of surface ring cracks.

Indentation stress-strain curves of individual layer Si_3N_4 materials used in this study for the coating or substrate layer were plotted in Fig. 3. In this figure, the indentation load, P_Y, at which a permanent surface impression below the contact load was first detected by Nomarski illumination was used to determine yield stress Y from equation (1).

$$P_Y/a^2=1.1Y \tag{1}$$

In the domain of small loads where the stress-strain curves are linear proportional, Young's modulus can be calculated from equation (2) (Swain and Lawn, 1969).

$$P_o=(3E/4\pi k)(a/r) \tag{2}$$

with $k=(9/16)[(1-\nu^2)+(1-\nu'^2)E/E']$ a dimensionless coefficient, E and ν, E' and ν' Young's modulus and Poisson's ratio of the material and spherical indenter respectively. In our analysis of indentation stress-strain curves, it allows each material to deform according to a modified critical shear stress condition (Fischer-Cripps and Lawn, 1996).

$$\sigma=E\varepsilon \quad (\sigma\leq Y) \tag{3}$$

$$\sigma=Y+\alpha(\varepsilon E-Y) \quad (\sigma\geq Y) \tag{4}$$

with α a dimensionless strain-hardening coefficient in the range $0\leq\alpha\leq1$ ($\alpha=1$, fully elastic; $\alpha=0$, fully plastic). While the individual layer materials used in the hard Si_3N_4 coated soft Si_3N_4 system ($E_c/E_s=1.06$) showed similar indentation stress-strain curve as shown in Fig. 3(a), the materials used in the Si_3N_4 coated Si_3N_4+BN system ($E_c/E_s=1.15\sim2.69$) showed different indentation stress-strain curve. The graphs of the Si_3N_4 and Si_3N_4+BN materials in the Fig. 3(b) foreshadow the elastic/plastic mismatch will be produced during the fabrication of bilayer basing on the discrepancy of slopes in the elastic and plastic region. Especially, the deviation from linearity indicates the material becomes 'soft' and 'quasi-plastic' in the local area around the surface as the amount of BN material increased in Si_3N_4, which is particular result in the stiff ceramic material because the fracture occurs in the elastic region in many brittle ceramics. The earlier studies show that effective "ductile" response can occur in the ceramics by distributed intergranular microfractures in a region of high shear stresses

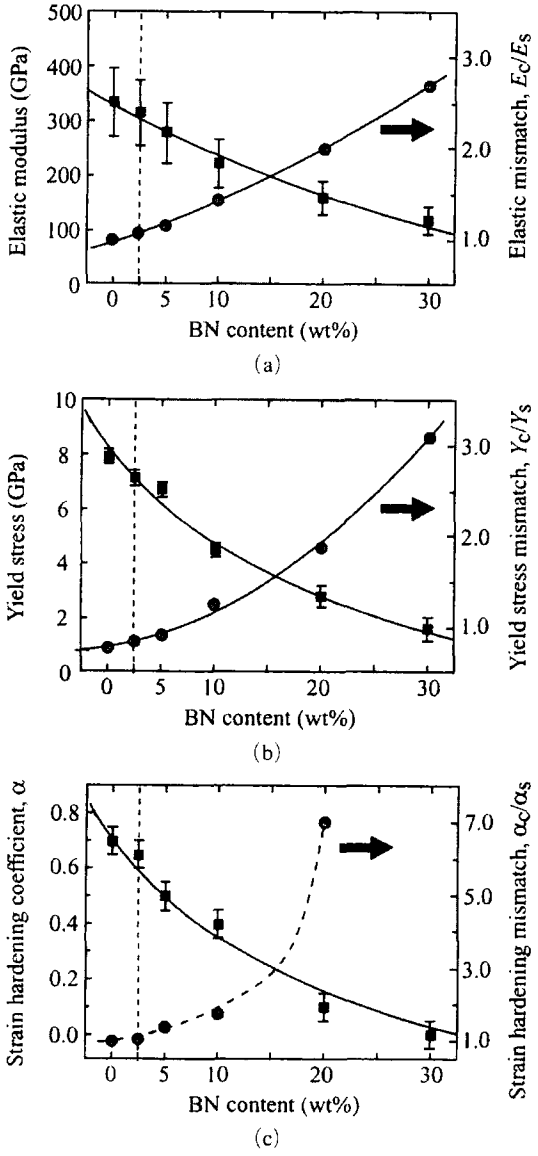

Fig. 4 Elastic and plastic properties of Si_3N_4 and Si_3N_4+BN composites as a function of BN content : (a) elastic modulus, (b) yield stress, and (c) strain hardening coefficient. Elastic/plastic mismatch was inserted in each graph. The data on the dotted lines indicate the data of hard Si_3N_4 on soft Si_3N_4

below the contact circle (Lawn et. al., 1994 ; Lee et. al., 1997).

The Elastic modulus, E, yield stresses, Y, strain hardening coefficients, α, of each layer materials obtained from Eq. (1) ~ (4) in the graph of Fig. 3 were plotted as a function of BN content in Fig. 4. The data on the dotted line correspond to that of soft Si_3N_4 used in the hard Si_3N_4 on soft Si_3N_4 material. All properties such as elastic modulus, yield stress and straining hardening coefficient decreased as the BN was added in the Si_3N_4 material as shown in the graphs. When the bilayer was fabricated, mismatch will be produce because of the different properties between the coating and the substrate layer. Elastic modulus mismatch, E_c/E_s where c and s subscripts are coating and substrate, affects the fracture behavior during the contact test when the ratio of elastic modulus are different in two layer materials. Likewise the plastic mismatch has an influence on the contact fracture in the plastic region of the indentation stress-strain curve. Each calculated mismatch, E_c/E_s, Y_c/Y_s, and α_c/α_s are inserted in each graph of Fig. 4. The mismatch values increase as the amount of BN addition increases in the Si_3N_4 substrate. The data of elastic modulus mismatch in the Si_3N_4 materials are also summarized in Table 1.

Figure 5 shows the micrographs of cracks corresponds to initiation and propagation in the hard Si_3N_4 coating layer on soft Si_3N_4. Coating thickness is controlled by 180 μm, and crack was induced using the same WC ball with radius of 1.98 mm at increasing load. In the hard Si_3N_4 on soft Si_3N_4, only cone cracks are found from the surface during the contact. The micrographs indicate that cone crack is initiated at load around $P=2000$ N (Fig. 5(a)) and propagated to the interface at $P=3000$ N (Fig. 5(b)).

Figure 6 shows the effect of coating thickness on the cone crack initiation load in the hard Si_3N_4 on soft Si_3N_4. Contact cracking is not sensitive to the coating thickness except the thinnest thickness, $d<50$ μm. Because there is not large elastic/plastic mismatch, $E_c/E_s=1.06$, in this bilayer, the initiation of the contact crack is not affected by coating thickness from 50 to 200 μm. The result indicates the coating thickness effect in the coating system with little elastic/plastic mismatch does not change a contact stress field (Lawn, 1993). According to Auerbach's law, the

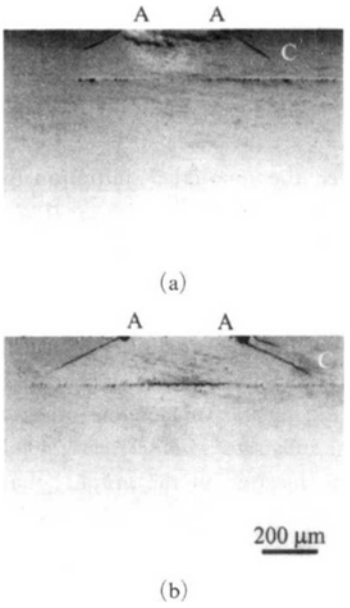

Fig. 5 Section views of contact damage in hard Si_3N_4 on soft Si_3N_4 with coating thickness $d=180$ μm, showing (a) initiation at $P=2000$ N and (b) propagation of contact cracks at $P=3000$ N, using WC sphere radius $r=1.98$ mm. Contact diameter AA indicated

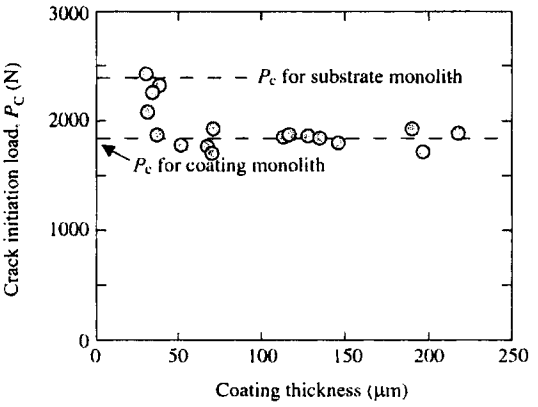

Fig. 6 Critical loads for contact crack initiation as function of coating thicknesses in hard Si_3N_4 on soft Si_3N_4. Dotted lines represent P_c of the coating and the substrate monolithic material, respectively

initiation of load of cone crack is function of material toughness, effective modulus and the radius of sphere indenter,

$$P_c = A(T^2/E')\,r \tag{5}$$

with $A = A(\nu)$ a dimensionless coefficient (ν is Poisson's ratio), T is the toughness (K_{IC}) and E' is an effective modulus, $E' = 1/(1/E + 1/E_i)$, where E_i is an elastic modulus of sphere indenter.

However, the cone crack initiation load value is beginning to rise when the coating thickness is less than 40 μm. It is thought that the substrate contributes the suppression of crack initiation from this thickness range. Our earlier result showed that the possibility of crack suppression by the soft substrate at thinly coated material (Lee et. al., 2000). In fact, the crack initiation load of the substrate is higher, $P_c = 2400$ N (upper dotted line inserted in the graph), than that of the coating layer monolith, $P_c = 1800$ N (lower dotted line in the graph).

On the other hand, in the Si_3N_4 on Si_3N_4+BN, which has larger elastic/plastic mismatch ($E_c/E_s = 1.44 \sim 2.69$) between the coating and the substrate layers, crack is initiated as a transverse crack from the interface at much lower load, at $P = 800$ N, as shown in Fig. 7(a). In this case, crack is not initiated from the surface at the first time. After the growth of transverse crack (M) is suppressed beneath the surface (contact region), cone crack (C) has appeared from the surface as shown in Fig. 7(b). Two peaks with high intensity appear in the acoustic emission detector when these two kinds of cracks are initiated at each critical load during the contact.

The data in Fig. 8 corresponds to the first peak in the acoustic emission detector during the contact on the bilayer materials using various substrates summarized in Table 1. All fracture initiates at lower load rather than P_c for coating monolith from the lower coating surface (M). In all case, only the elastic modulus mismatch is important because the yield stress of coating material is higher than the stress corresponding to the critical load. For an infinitely wide center-point-loaded coating on a compliant substrate in the limit of small contacts ($a \ll d$) and surface displacements (Timoshenko and Woninowsky-

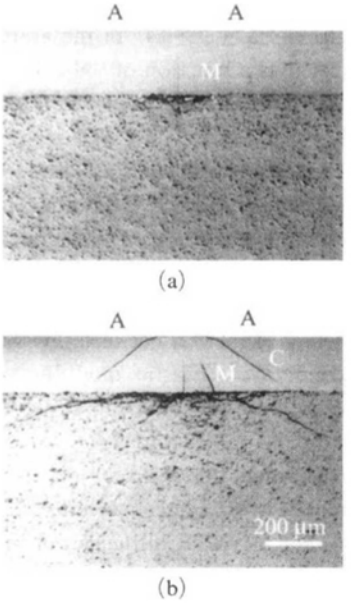

Fig. 7 Section views of contact damage in Si_3N_4 on Si_3N_4+30wt% BN with coating thickness $d = 250$ μm, showing (a) initiation at $P = 800$ N and (b) propagation of contact cracks at $P = 1000$ N, using WC sphere radius $r = 1.98$ mm. Contact diameter AA indicated

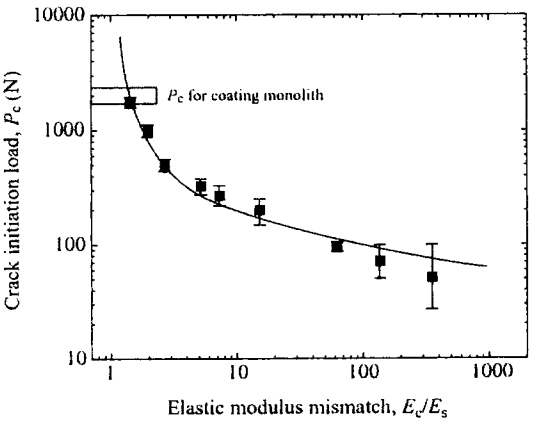

Fig. 8 Plot of critical loads for transverse crack produced using WC sphere radius $r = 1.98$ mm versus E_c/E_s for Si_3N_4 coatings on various substrates of different modulus summarized in Table 1. The coating thickness of silicon nitride was fixed for 250 μm

Krieger, 1959),

$$P_c = B\sigma_F d^2/\log(CE_c/E_s) \qquad (6)$$

with coating thickness, d, strength of coating material, σ_F, and B and C dimensionless coefficients. The solid curve is the best fit for $B=3.378$ and $C=0.891$ obtained by inserting $d=250\ \mu m$ and $\sigma_F=900$ MPa.

Plot such as Fig. 8 exhibits sensitivity of contact fracture to E_c/E_s (at $E_c/E_s>1.44$). The decline of P_c at more compliant substrate indicates hard ceramic coatings should be carefully designed. Particularly, the fracture mode at the bottom surface of the coating below the contact is dangerous because they remain subsurface and is not detected in opaque coatings. The controlling material parameters are strength and thickness of coating layer as indicated in Eq. (6).

Typical FEM-generated contours of principal stresses in the Si_3N_4 on Si_3N_4+BN are shown in Fig. 9(a). Principal stresses at shaded areas correspond to tensile zones ($\sigma_1 \geq 0$) and white areas indicate compressive zones. The initiation of transverse crack (M) as shown in Fig. 7(a) correlates strongly with the region of the highest tensile stress immediately above the interface between the coating and the substrate layer. A high elastic modulus mismatch moves the region that crack is initiated from the *surface* into *interface*. The secondary largest stresses are located in the surface region (C). Therefore it is bending stress to dominate the damage patterns in the coating layer during the Hertzian contact test because the underlayer is relatively softer (Pajares et al., 1996a; Pajares et al., 1996b). The maximum tensile stress in the FEM-generated contour was plotted as a function of elastic modulus mismatch in the Si_3N_4 on Si_3N_4+BN with coating thickness $d=250\ \mu m$, using WC sphere $r=1.98$ mm at $P=2000$ N. The maximum stress in the interface is very sensitive to the elastic modulus mismatch while the surface is not. The maximum stress increased at the interface lowers the initiation load of transverse cracks. Therefore high tensile stress in the interface causes the crack initiation easily at lower load as shown in Fig. 8 when the mismatch increases in the hard coating layer on soft materials.

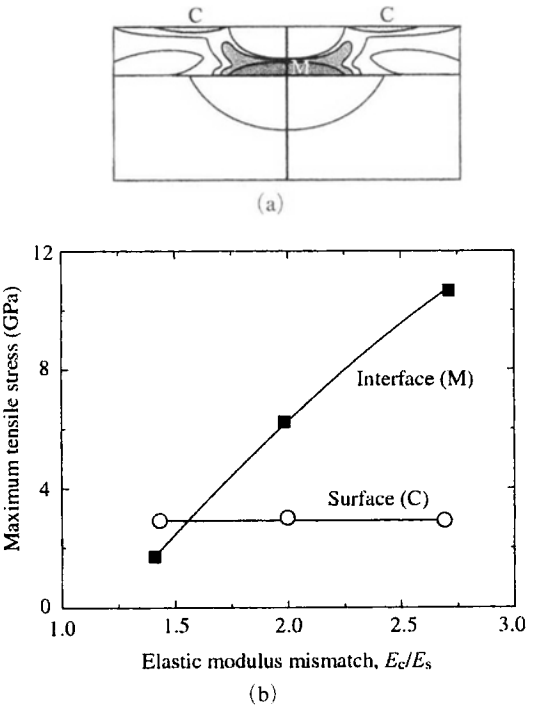

Fig. 9 The stress contour and the maximum stress versus E_c/E_s for Si_3N_4 on Si_3N_4+BN with coating thickness $d=250\ \mu m$, using WC sphere $r=1.98$ mm at $P=2000$ N. (a) FEM-generated principal normal stress in the Si_3N_4 on Si_3N_4+20 wt%BN, shading indicating tensile zones ($\sigma_1 \geq 0$), white areas indicating compressive zones. (b) Maximum principal tensile stresses in the interface and surface regions during the contact test

In this hard coating system, coating layer thickness becomes an important controllable variable in designing for crack suppression (Pajares et al., 1996a; Pajares et al., 1996b). A different coating thickness changes the stress fields to affect the fracture and damage modes. Figure 10 shows the effect of coating thickness on the crack initiation load in the Si_3N_4 on Si_3N_4+30 wt%BN ($E_c/E_s=320/119=2.69$), using WC sphere $r=1.98$ mm at $P=2000$ N. Filled symbols are for transverse cracking and the solid lines are the corresponding predictions from Eq. (6). The dotted line is limit of contact experiment. The agreement between data and solid curve suggests a

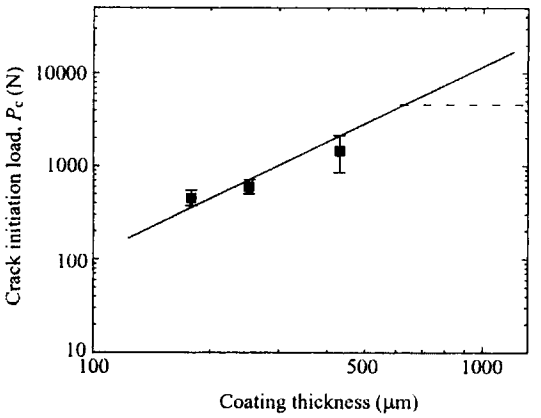

Fig. 10 Critical loads for contact crack initiation as function of coating thicknesses in Si_3N_4 on Si_3N_4+30wt%BN with coating thickness d=250 μm, using WC sphere r=1.98 mm at P=2000 N

significant influence of the coating thickness, d, on the initiation of transverse crack, P_c. The result shows that thicker coating prolongs the initiation of contact cracks. In other words, when the elastic/plastic mismatch is larger between the coating and substrate layer, as it causes the contact cracks at lower crack initiation load, P_c, particularly at the interface, the coating thickness should be increased.

4. Conclusion

(1) In this study, elastic modulus mismatch, E_c/E_s, were varied from 1.06 to 356 by changing the soft substrate material with hard silicon nitride coatings. Hertzian contact test is conducted for producing contact cracks and the acoustic emission detecting technique for measuring the critical load of crack initiation.

(2) The larger the elastic/plastic mismatch between the coating and the substrate layers, the initiation of cracks occurred at lower load during the contact, from the interface between the coating and the substrate layer because of flexural stress of the coating layer on soft compliant substrate. On the other hand, the crack initiation occurs from the surface in the smaller mismatch ($E_c/E_s<1.44$).

(3) Equations 5 and 6 provide a basis for designing against contact fracture in the hard coating layer structures. The material parameters that govern the critical initiation loads for the hard coating structures with larger mismatch are the coating thickness, d and the strength of coating material, σ_F.

References

Bartlett, A. H. and Maschio, R. D., 1995, "Failure Mechanisms of a Zirconia-8 wt% Yttria Thermal Barrier Coating," *Journal of the American Ceramic Society*, Vol. 78, pp. 1018~1024.

Evans, A. G. and Hutchinson, J. W., 1984, "On the Mechanics of Delamination and Spalling in Compressed Films," *Int. J. Solids Struct.*, Vol. 20, No. 5, pp. 455~466.

Fischer-Cripps, A. C. and Lawn, B. R., 1996, "Stress Analysis of Contact Deformation in Quasi-Plastic Ceramics," *Journal of the American Ceramic Society*, Vol. 79, No. 10, pp. 2609~2618.

Frank, F. C. and Lawn B. R., 1967, "On the Theory of Hertzian Fracture," *Proc. R. Soc.*, London, Vol. A299, pp. 291~306.

Hertz, H., 1896, *Miscellaneous papers*, Macmillan, London, Chaps. 5 and 6.

Hutchinson, J. W. and Suo, Z., 1991, "Mixed-Mode Cracking in Layered Structures," *Adv. Appl. Mech.*, Vol. 29, pp. 1991~1998.

Jin, S. B. and Kim, S. S., 2000, "A Simplified Estimation of Stress Intensity Factor on the Hertzian Contact," *KSME International Journal*, Vol. 1, pp. 8~11.

Kim, S. S., Ahn, C. W. and Kim, T. H., 2002, "Tribological Characteristics of Magnetron Sputtered MoS_2 Films in Various Atmospheric Conditions," *KSME International Journal*, Vol. 16, pp. 1065~1071.

Knight, J. C., Page, T. F. and Hutchings, I. M., 1989, "The Influence of Substrate Hardness on the Response of TiN-Coated Steels to Surface Deformations," *Thin Solid Films*, Vol. 177, pp. 117~132.

Lawn, B. R., 1993, *Fracture of Brittle Solids*, Cambridge University Press, Cambridge.

Lawn, B. R., Padture, N. P., Cai, H. and Guiberteau, F., 1994, "Making Ceramics "Ductile"," Science, Vol. 263, pp. 1114~1116.

Lee, K. S., Park, J. Y., Kim, W. J., Lee, M. Y., Jung, C. H. and Hong, G. W., 2000, "Effect of Soft Substrate on the Indentation Damage in Silicon Carbide Deposited on Graphite," *Journal of Materials Science*, Vol. 35, pp. 2769~2777.

Lee, S. K., Wuttiphan, S. and Lawn, B. R., 1997 "Role of Microstructure in Hertzian Contact Damage in Silicon Nitride : I. Mechanical Characterization," *Journal of the American Ceramic Society*, Vol. 80, No. 9, pp. 2367~2381.

Pajares, A., Wei, L., Lawn, B. R. and Berndt, C. C., 1996a, "Contact Damage in Alumina-Based Plasma Sprayed Coatings," *Journal of the American Ceramic Society*, Vol. 79, No. 7, pp. 1907~1914.

Pajares, A., Wei, L., Lawn, B. R., Padture, N. P. and Berndt, C. C., 1996b, "Mechanical Characterization of Plasma Sprayed Ceramic Coatings on Metal Substrates by Contact Testing," *Materials Science and Engineering*, Vol. A208, pp. 158~165.

Seo, D. W. and Lim, J. K., 2002, "Effects of Strain Rate and Temperature on Fracture Strength of Ceramic/Metal Joint Brazed with Ti-Ag-Cu Alloy," *KSME International Journal*, Vol. 16, pp. 1078~1083.

Swain, M. V. and Lawn, B. R., 1969, "A Study of Dislocation Arrays at Spherical Indentations in LiF as a Function of Indentation Stress and Strain," *Physica Status Solidi*, Vol. 35, No. 2, pp. 909~923.

Swain, M. V. and Mencik, J., 1994, "Mechanical Property Characterization of Thin Films Using Spherical Tipped Indenter," *Thin Solid Films*, Vol. 253, pp. 204~211.

Timoshenko, S. and Woinowsky-Krieger, S., 1996, *Theory of Plates and Shells*, McGraw-Hill, New York, Chap. 8.

Wuttiphan, S., Lawn, B. R. and Padture, N. P., 1996, "Crack Suppression in Strongly-bonded Homogeneous/Heterogeneous Laminates : A Study on Glass/Glass-Ceramic Bilayers," *Jornal of the American Ceramic Society*, Vol. 79, pp. 634~640.